ACS APPLIED MATERIALS & INTERFACES

Research Article

www.acsami.org

"Rocking-Chair"-Type Metal Hybrid Supercapacitors

Hyun Deog Yoo,[*,†,‡] Sang-Don Han,[‡,§] Ryan D. Bayliss,[†,‡] Andrew A. Gewirth,[‡,∥] Bostjan Genorio,[‡,⊥,#] Nav Nidhi Rajput,[‡,▽] Kristin A. Persson,[‡,▽,○] Anthony K. Burrell,[‡,§] and Jordi Cabana[*,†,‡]

[†]Department of Chemistry, University of Illinois at Chicago, Chicago, Illinois 60607, United States

[‡]Joint Center for Energy Storage Research, Argonne National Laboratory, Argonne, Illinois 60439, United States

[§]Chemical Sciences and Engineering Division, Argonne National Laboratory, Argonne, Illinois 60439, United States

[∥]Department of Chemistry, University of Illinois at Urbana−Champaign, 600 S. Mathews Avenue, Urbana, Illinois 61801, United States

[⊥]Materials Science Division, Argonne National Laboratory, Argonne, Illinois 60439, United States

[#]University of Ljubljana, Faculty of Chemistry and Chemical Technology, Vecna pot 113, 1000 Ljubljana, Slovenia

[▽]Environmental Energy Technology Division, Lawrence Berkeley National Laboratory, Berkeley, California 94720, United States

[○]Department of Materials Science and Engineering, University of California, Berkeley, California 94720-1760, United States

ABSTRACT: Hybrid supercapacitors that follow a "rocking-chair"-type mechanism were developed by coupling divalent metal and activated carbon electrodes in nonaqueous electrolytes. Conventional supercapacitors require a large amount of electrolyte to provide a sufficient quantity of ions to the electrodes, due to their Daniell-type mechanism that depletes the ions from the electrolyte while charging. The alternative "rocking-chair"-type mechanism effectively enhances the energy density of supercapacitors by minimizing the necessary amount of electrolyte, because the ion is replenished from the metal anode while it is adsorbed to the cathode. Newly developed nonaqueous electrolytes for Mg and Zn electrochemistry, based on bis(trifluoromethylsulfonyl)imide (TFSI) salts, made the metal hybrid supercapacitors possible by enabling reversible deposition on the metal anodes and reversible adsorption on an activated carbon cathode. Factoring in gains through the cell design, the energy density of the metal hybrid supercapacitors is projected to be a factor of 7 higher than conventional devices thanks to both the "rocking-chair"-type mechanism that minimizes total electrolyte volume and the use of metal anodes, which have substantial merits in capacity and voltage. Self-discharge was also substantially alleviated compared to conventional supercapacitors. This concept offers a route to build supercapacitors that meet dual criteria of power and energy densities with a simple cell design.

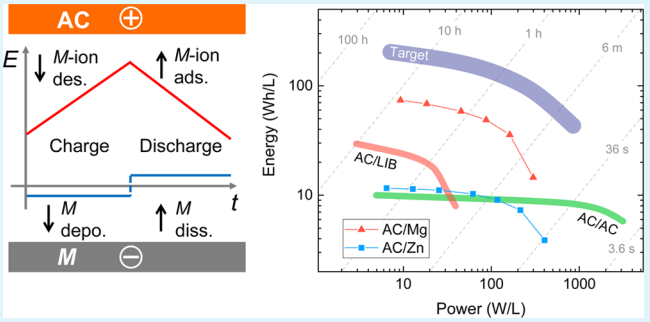

KEYWORDS: *supercapacitors, energy density, "rocking chair"-type mechanism, metal anodes, volume of electrolyte, self-discharge*

INTRODUCTION

Cheap, efficient, and reliable energy storage devices can help balance and regulate intermittent and distributed renewable energy sources.[1] Among many energy storage devices, supercapacitors can store pulse power efficiently because of their high rate capability and long-term cyclability. The origin of this efficiency is their simple mechanism of operation that is based on the adsorption and desorption of ions on the surface of porous electrodes.[2] It is possible to charge or discharge supercapacitor cells in minutes for over a half million cycles without substantial performance degradation.[3] On the basis of their high power characteristics, supercapacitors can assist batteries or fuel cells proposed for electric vehicles and electricity grids to release and harness peak power surges.[4] However, wide application of such devices has been hindered in part due to the low energy density currently achievable, which stems from the symmetric configuration of activated carbon (AC) as the positive and negative electrodes (Figure 1a). First, the specific capacitance of the cell is 25% of the electrode's capacitance; the serial connection of two identical electrodes makes the total capacitance half the value of either one, while the total mass is doubled.[5] Second, conventional supercapacitors follow a Daniell-type mechanism,[6] where ions are depleted from the electrolyte upon charge and replenished to the electrolyte upon discharge (Figure 1a). In this mechanism, the electrolyte serves as an ionic reservoir, from which cations and anions are supplied to negative and positive electrodes, respectively. Consequently, substantial volume of electrolyte is required for Daniell-type cell to function properly.[7−10] The requirement of ionic reservoir leads to severe limitations in the

Received: July 8, 2016
Accepted: October 24, 2016
Published: October 24, 2016

DOI: 10.1021/acsami.6b08367
ACS Appl. Mater. Interfaces 2016, 8, 30853−30862

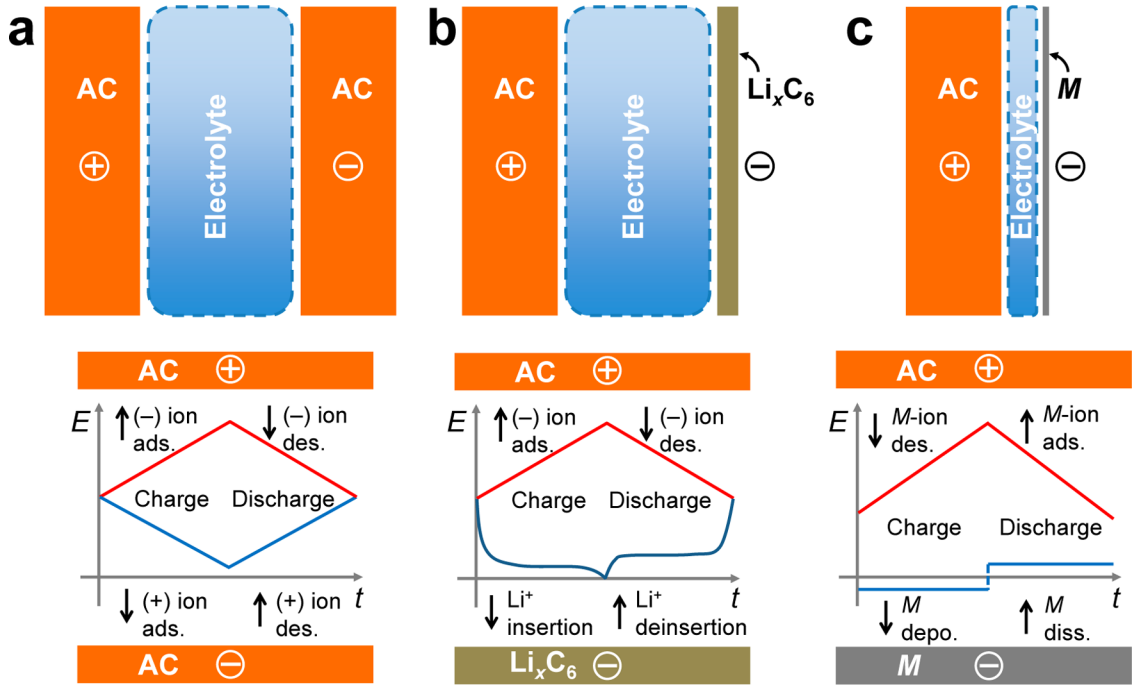

Figure 1. Scheme (top) and mechanism (bottom) for (a) AC/AC symmetric, (b) AC/graphite hybrid, and (c) AC/metal hybrid capacitors, highlighting the features of (a, b) Daniell-type and (c) rocking-chair-type mechanisms, respectively.

energy density attainable by the supercapacitor and to an increase in the internal resistance during charging due to depletion of salts in the electrolyte.[11]

Hybrid supercapacitors (Figure 1b) substitute one of the supercapacitor electrodes with a battery electrode such as lead dioxide (PbO_2), nickel oxyhydroxide (NiO(OH)), lithiated graphite (Li_xC_6), lithium titanate ($Li_4Ti_5O_{12}$), transition metal oxides, electroactive polymers, or lithium manganese oxide ($LiMn_2O_4$).[12−21] A hybrid supercapacitor that utilizes a Mg metal anode has been suggested,[5] but addition of Li salt was required as the Mg organo-haloaluminate complex ions in the electrolyte were too large to be adsorbed on the AC electrode. These alternative approaches can enhance the energy density of the cell versus the traditional supercapacitor cell design (i.e., AC/AC), because the battery electrode provides a large specific capacitance (it is semi-infinite compared to the activated carbon) and higher voltage (Figure 1b). However, the energy density is still limited by the volume of electrolyte since the cell is still based on the Daniell-type mechanism of charge transport, which depletes the electrolyte on charging (Figure 1b).

In this paper, we introduce a metal hybrid supercapacitor that follows a "rocking-chair"-type mechanism. This hybrid supercapacitor is composed of a metal negative electrode[22,23] and an activated carbon positive electrode (Figure 1c). Recently developed nonaqueous electrolytes for Zn and Mg based on bis(trifluoromethylsulfonyl)imide (TFSI) salts enable this construct,[24−27] as these electrolytes permit both metal deposition/dissolution and metal-ion adsorption/desorption in an electrolyte solution. According to the "rocking-chair"-type mechanism,[28] upon discharge of a cell, the metal (M) anode dissolves giving the M^{n+} ions to the solution, which are transferred into and adsorbed on the pores of the AC cathode, while upon charge, the cathode expels the adsorbed M^{n+} ions, which are transferred to and deposited on the metal anode (Figure 1c). As a result, only a minimum amount of electrolyte is required to operate the cell since the electrolyte serves only to transport M^{n+} ions. The use of metal electrodes further increases the energy densities at the cell level, due to their high intrinsic volumetric capacity (e.g., 3837 and 5853 Ah L^{-1} for Mg and Zn, respectively). In addition, the self-discharge was substantially alleviated compared to conventional supercapacitors because the mechanism of operation pins the maximum potential of the AC cathode close to the point of zero charge (pzc). Therefore, the "rocking-chair"-type metal hybrid supercapacitors provide a fundamental solution to the low energy density and severe self-discharge of conventional supercapacitors, which are their most pressing issues.

EXPERIMENTAL SECTION

Preparation of Electrolytes. Zinc bis(trifluoromethylsulfonyl)-imide ($Zn(TFSI)_2$, Solvionic, 99.5%) salt was dried in a vacuum oven at 125 °C and mixed with anhydrous acetonitrile (Sigma-Aldrich, 99.8%) in hermetically sealed glass vials and stirred to form a homogeneous solution of 0.5 M $Zn(TFSI)_2$ in acetonitrile.[27] Magnesium bis(trifluoromethylsulfonyl)imide ($Mg(TFSI)_2$, Solvionic, 99.5%) and magnesium chloride ($MgCl_2$, Sigma-Aldrich, 99.99%) salts were used after drying at 150 °C in a vacuum oven. Diethylene glycol dimethyl ether (diglyme or G2, Sigma-Aldrich, spectrophotometric grade) was dried over activated basic Al_2O_3, filtered, and vacuum distilled over liquid Na/K alloy using a Vigreux column. The 0.3 M $Mg(TFSI)_2$ and 0.15 M $MgCl_2$ were mixed together with diglyme in hermetically sealed glass vials and stirred to form homogeneous solutions. Addition of $MgCl_2$ was critical for reversible Mg deposition/dissolution, either because of the formation of active species such as $MgCl^+$ or $Mg_2Cl_3^+$[26,29] or due to the modification of the electrode−electrolyte interface by the adsorption of free chloride ions.[26,30] Then, the electrolyte solution was further dried by molecular sieves. All-phenyl-complex (APC) electrolyte was prepared by carefully adding 0.8 M phenylmagnesium chloride into 0.4 M $AlCl_3$ in tetrahydrofuran (THF), as described elsewhere.[31] Lithium chloride (LiCl) was added to APC solution until it was saturated, at 0.4−0.5 M, to prepare an APC electrolyte containing Li-ions. Note that only ethereal solvents (e.g., diglyme or THF) can be used for Mg hybrid supercapacitors

DOI: 10.1021/acsami.6b08367
ACS Appl. Mater. Interfaces 2016, 8, 30853−30862

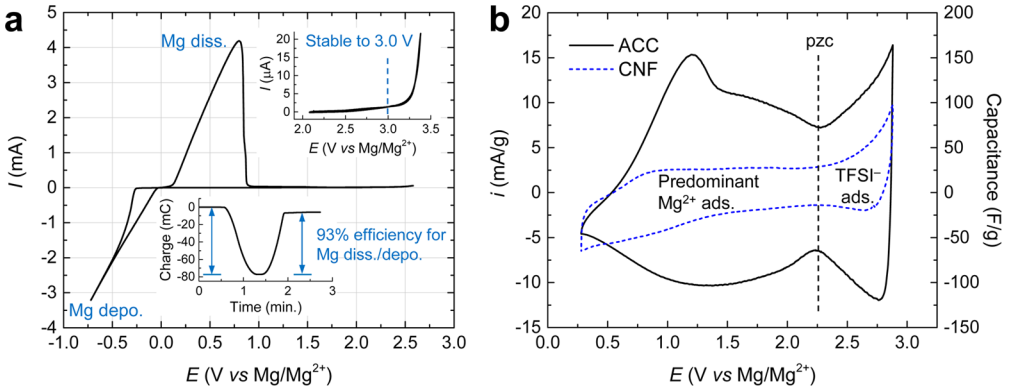

Figure 2. (a) Cyclic voltammogram on Pt collected at 25 mV s^{-1}. (b) Cyclic voltammograms of microporous carbon (ACC, black line) and mesoporous carbon (CNF, blue dash) as the working electrodes in a TFSI-based electrolyte at 0.1 mV s^{-1}. Different scan rates were used for Pt and AC electrodes because of the different characteristic time (or response time) of the electrodes: a few milliseconds and a few hundred seconds for Pt and AC electrodes, respectively.

because other kinds of solvents (e.g., acetonitrile or carbonates) are reduced on the surface of Mg metal, forming a passivation film that is insulating toward Mg^{2+} ions.[32] All materials were handled in an Ar-filled glovebox (<0.5 ppm of H_2O and <0.5 ppm of O_2). The water content of the electrolytes was verified to be <30 ppm using a Mettler Toledo DL39 Karl Fischer coulometer. Ionic conductivity was determined by measuring the impedance of the electrolytes in a homemade two electrode cell at 25 °C.[33] At least three measurements were made with a fresh sample after each analysis.

Preparation of Electrodes. An activated carbon cloth (ACC-5092-20, Kynol Co., surface area = 2000 m^2 g^{-1}) was dried at 80 °C under vacuum overnight and used as the cathode. The activated carbon cloth was punched to a circle with an area of 1.0 cm^2 and corresponding mass of 15.1 mg. Carbon nanofoam (Grade I, Marketech Intl Inc., surface area = ~400 m^2 g^{-1}) paper was used for mesoporous carbon aerogel. For the metal electrode, a magnesium foil (99.95%, GalliumSource LLC, 50 μm thick) or a zinc foil (99.98%, Alfa Aesar, 250 μm thick) was abraded inside the glovebox to expose a fresh metal surface.

Electrochemical Measurements. Electrochemical characterization was performed using custom-made 3-electrode glass cells or 2032 coin-type cells. For the 3-electrode cell test, a piece of activated carbon cloth (ACC) attached to a platinum wire was used as the working electrode and metal foils served as both counter and reference electrodes. The three electrodes were introduced in a hermetically sealed glass cell that contains ca. 5 mL of electrolyte. In the coin-type cells, the ACC cathode and metal anode were separated with a microporous membrane made with polypropylene (Celgard 2400, 25 μm thick) and a glass fiber membrane (grade 691, VWR Co., 210 μm thick). The amount of electrolyte in the coin cells was ca. 200 μL unless otherwise specified. Cyclic voltammetry, galvanostatic, and impedance measurements were performed using a galvanostat/potentiostat (VMP3, Biologic Co.) at room temperature. It was found that the potential of Mg reference electrode shifts to about 0.1 V higher than Mg/Mg^{2+} due to formation of a passivation layer on its surface, which happens spontaneously upon immersion into the electrolyte. Similar phenomena were observed in a previous study of a calcium-ion electrolyte.[34] Therefore, the electrode potentials were corrected with respect to the open circuit potential of the Mg counter electrode with a freshly exposed Mg surface immediately after the Mg deposition or stripping.

Molecular Dynamics (MD) Simulations. Classical MD simulations are performed using GROMACS MD simulation package version 5.1.2.[35] The initial structures with periodic boundary conditions in *XYZ* directions are prepared using PACKMOL. All systems are first minimized using the steepest descent followed by conjugated-gradient energy minimization scheme. We first performed NPT simulations for 2 ns followed by heating the systems in NVT at 400 K for 2 ns and then quenching to 298 K in 3 ns. The cluster size in each case is obtained using the final production runs in NVT ensemble with 10 ns long trajectories. Force field parameters and other simulation details closely follow that described in our previous publications.[27,36]

Calculation of Energy and Power Densities. The specific energy (Wh kg^{-1}) and energy density (Wh L^{-1}) were calculated following a method reported in the literature.[7,8] Energy (E) was calculated by integrating the voltage profile ($E = \int V dQ$ in voltage (V) vs charge (Q) curve) of each cell. Then, the energy was divided by the total mass (m_{tot}) or volume (v_{tot}) of the cell to give specific energy or energy density, respectively. The total mass and volume of the cell was calculated assuming an ideal cell that comprises electrodes and electrolyte only, without peripherals such as cases and separators. In all calculations, the mass of AC electrode (m_+) was set to 1 g for simplicity. In a symmetric AC/AC capacitor, the mass of the anode (m_-) is also 1 g. For the asymmetric AC/LIB and AC/M (M is metal, e.g., Mg) cells, the mass of anode is given as $m_- = \frac{Q_+}{Q_{-,sp}}$, where Q_+ is the specific capacity of the cathode and $Q_{-,sp}$ is the specific capacity of the anode. For Daniell-type cells, the volume of electrolyte (v_i) was calculated as $v_i = \frac{3Q_+}{czF}$, where c is the concentration of the electrolyte (e.g., 1 M for AC/AC and AC/LIB), z is the charge of the ion (e.g., +1 for Li^+), and F is Faraday constant (96 485 C mol^{-1}). We add a multiplier of 3 to the minimally required volume, $\frac{Q_+}{czF}$, to account for the excess of electrolyte needed to maintain 80% ionic conductivity at the point of highest ion storage in the electrodes.[37] In the case of the rocking-chair-type cells, the minimum volume of electrolyte is the pore volume of AC electrode (V_{pore} = 0.69 cm^3/g), which must be filled with electrolyte for the double-layer charging. The interconversion between mass and volume used the reported density values of electrolyte (1.2 g cm^{-3}),[8] carbon (2.2 g cm^{-3}), Mg (1.74 g cm^{-3}), Zn (7.14 g cm^{-3}), and Li (0.534 g cm^{-3}).[38] Then, m_{tot} and v_{tot} is given as $m_{tot} = m_+ + m_- + m_i$ and $v_{tot} = v_+ + v_- + v_i$. The relationship between energy and power (i.e., the Ragone plot) was estimated from the experimental rate performance data, either from this work for AC/Mg and AC/Zn cells or from the literature for AC/AC and AC/LIB cells.[39,40]

RESULTS AND DISCUSSION

The cyclic voltammogram of the Mg^{2+} electrolyte on a Pt electrode shows reversible Mg deposition/stripping with Coulombic efficiency of 93% and an overpotential of 0.26 V (Figure 2a and the lower inset).[25,26] The anodic limit of stability is approximately 2.5−3.0 V vs Mg/Mg^{2+} as shown in the upper inset of Figure 2a. The ACC electrode was electrochemically characterized in the same cell (Figure 2b). It exhibits a capacitance of about 100 F g^{-1} at 1.0−2.9 V vs Mg/

DOI: 10.1021/acsami.6b08367
ACS Appl. Mater. Interfaces 2016, 8, 30853−30862

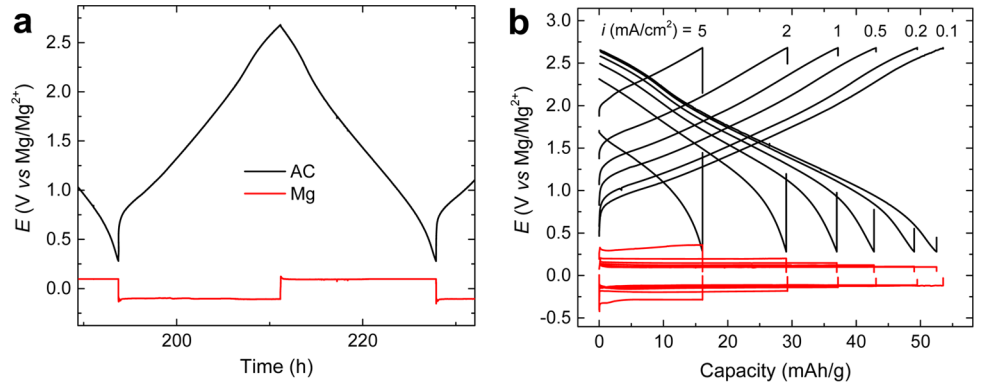

Figure 3. Galvanostatic charge−discharge profiles collected in a 3-electrode full cell: (a) at 50 μA cm^{-2} and (b) at varied current density from 0.1 to 5 mA cm^{-2}. The potential (E) of AC (black line) and Mg (red line) electrodes were traced simultaneously.

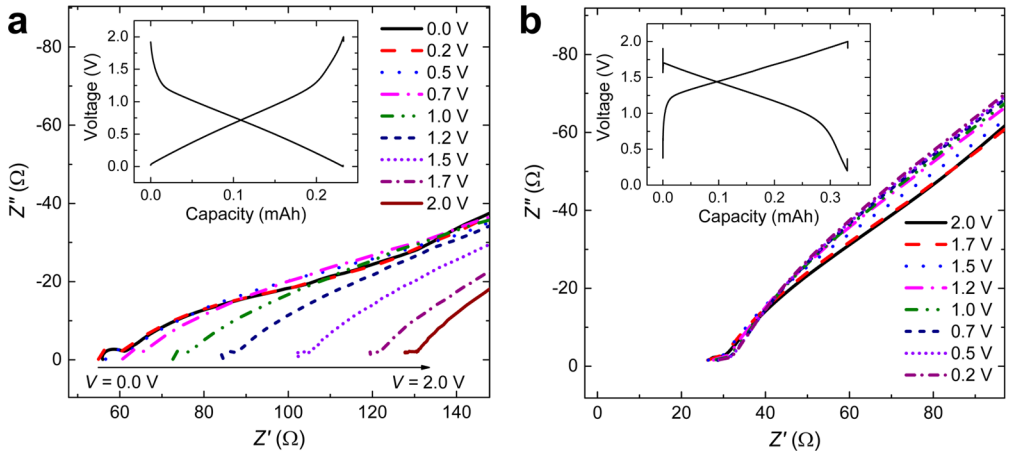

Figure 4. Electrochemical impedance collected at different applied voltages for (a) AC/AC symmetric and (b) AC/Mg hybrid cells. The insets depict a full galvanostatic cycle for these devices. The electrolyte for AC/AC cell was 0.3 M $Mg(TFSI)_2$ in diglyme.

Mg^{2+}. The voltammogram in Figure 2b exhibits a local minima at about 2.3 V vs Mg/Mg^{2+}, which corresponds to the point of zero charge (pzc).[41] Mg^{2+} ions are adsorbed/desorbed at potentials negative of the pzc, while the counteranions accumulate at potentials positive of the pzc. Interestingly, the capacitance plot of ACC in Figure 2b exhibits a local maximum at ca. 1.0 V, a feature not found when a mesoporous carbon aerogel (CNF) is utilized as the electrode. Voltage hysteresis at the low potentials in Figure 2b can be due to kinetic reasons, e.g., saturation or trapping of ions in the AC pores.[42,43] This feature is present even at the smallest charge/discharge rates (Figure 3a), suggesting a possible thermodynamic origin. We suggest the maximum in capacitance is associated with stronger adsorption of Mg^{2+} at potentials below ca. 1.0 V due to the presence of active sites, such as −OH, on the ACC. This behavior suggests that the operational voltage should be carefully selected to avoid possible hindrances. However, careful control of the ACC pore chemistry could also alleviate this apparent limitation.

The Mg hybrid supercapacitor cell was characterized by galvanostatic charge−discharge at 50 μA cm^{-2} (Figure 3a). The voltage profiles of both ACC and Mg electrodes were recorded simultaneously with respect to the reference electrode. The voltage profile of the ACC cathode exhibits a linear slope, which signifies the presence of nearly constant capacitance over the potential range from 0.7 to 2.7 V vs Mg/Mg^{2+}. The Mg metal anode shows a constant potential of approximately 0.0 V vs Mg/Mg^{2+} with an overpotential of 0.1 V for the deposition and stripping of Mg. Since the slope of the Mg deposition and stripping voltage profile is nearly zero, the specific capacitance approaches semi-infinity. The specific capacitance of a supercapacitor cell (C_{tot}) is given by the function of specific capacitance (C_+, C_-) and mass (m_+, m_-) of positive and negative electrodes according to the following equation:[5]

$$C_{tot} = \frac{m_+ m_-}{m_+ + m_-}\frac{C_+ C_-}{m_+ C_+ + m_- C_-} \quad (1)$$

In the case of a symmetric supercapacitor cell, where $C \approx C_+ \approx C_-$ and $m \approx m_+ \approx m_-$, the specific capacitance is 25% of each electrode's specific capacitance ($C_{tot} = 0.25\ C$). This means that only 25% of the electrode's capacitance is utilized at the cell level. On the other hand, the capacitance of a metal electrode can be regarded as infinitely large compared to the capacitance of activated carbon ($C_+ \ll C_-$). Thus, the total specific capacitance of a hybrid supercapacitor is $\frac{m_+}{m_+ + m_-}C_+$, which can be made close to the specific capacitance of the activated carbon (C_+) if the mass of Mg anode (m_-) is minimized by proper engineering. This strategy creates a path toward utilizing the full theoretical capacitance of the activated carbon electrode.

The rate capability of the Mg hybrid supercapacitor cell was analyzed by varying the current density from 0.1 to 5 mA cm^{-2} upon charge and discharge (Figure 3b). The capacitance of the

DOI: 10.1021/acsami.6b08367
ACS Appl. Mater. Interfaces 2016, 8, 30853−30862

ACC, which is the reciprocal of the slope in the galvanostatic voltage profile, is nearly constant at 90 F g^{-1} for various current densities within 2.6−1.5 V vs Mg/Mg^{2+}. However, at lower potentials (i.e., 1.5−0.3 V vs Mg/Mg^{2+}), the capacitance is significantly decreased at the higher current densities. The Mg metal anode shows flat voltage profiles near 0.0 V vs Mg/Mg^{2+} for all current densities. The overpotential is less than 0.15 V up to 0.1 mA cm^{-2} and increases to 0.35 V at 5 mA cm^{-2}. These results suggest that the Mg metal anode exhibits facile and reversible deposition/stripping kinetics under these conditions and, thus, can couple with a capacitive electrode at current densities as high as 2−5 mA cm^{-2}.

To demonstrate the advantage of the rocking-chair-type mechanism in the necessary volume of electrolyte, AC/AC and AC/Mg coin-type cells were fabricated using a limited volume of electrolytes. The Nyquist plots in Figure 4 show the changes in the impedance of the coin-type cells at different potentials for both the AC/AC symmetric and the AC/Mg hybrid configurations. In Figure 4, the resistance of the electrolyte is denoted by the x-abscissa value of the impedance (i.e., the real part of the impedance (Z') at the highest frequency), assuming a simplified Randles circuit model for the cell.[44] The amount of Mg^{2+} electrolytes was adjusted so that there was a 100% excess of Mg^{2+} relative to the amount required to fully charge or discharge the AC electrode. This amount of Mg^{2+} implies that the resistance of the electrolyte should become twice as great when the AC electrodes fully adsorb the ions. Indeed, Figure 4a shows that the electrolyte resistance increases by a factor of 2.3 (i.e., from 55 to 128 Ω) upon charging the AC/AC cell to 2.0 V. Conversely, the electrolyte's resistance is kept constant at about 28 Ω at different voltages of the AC/Mg hybrid cell (Figure 4b), as expected. This effect is a consequence of the Mg^{2+} ions adsorbed to the AC electrode being replenished by the Mg metal anode, so that the Mg^{2+} concentration is effectively kept constant. This observation supports the concept that the AC/Mg hybrid supercapacitor follows a "rocking-chair"-type mechanism for the operation of the cell. Practically, this fact creates a means to maximize the energy density of the hybrid supercapacitors by minimizing the amount of electrolyte, bypassing depletion of the ions in the electrolyte.[11]

The TFSI-based electrolyte enables superior device performance compared to conventional Grignard-based Mg electrolyte.[5,31,45] The TFSI-based electrolyte exhibits improved specific capacitance and a larger usable voltage window for the adsorption/desorption of Mg^{2+} ions relative to the Grignard-based electrolytes. Indeed, the carbon electrode in a Grignard-based electrolyte had a specific capacitance less than 79 F g^{-1}, with the voltammogram exhibiting little capacitance below 2.0 V vs Mg/Mg^{2+} as the pores were saturated by the relatively large ions.[5] In this case, addition of Li^+ to the electrolyte was required to increase the specific capacitance of the ACC, a consequence of which was that the cell then followed a Daniell-type mechanism.[5] The improved behavior of the TFSI-based electrolyte suggests that the solvated Mg^{2+} ions are significantly smaller, creating access to the small pores in the ACC. From the above results, the resulting Mg hybrid supercapacitor cell follows a "rocking-chair"-type mechanism if it is operated below the pzc, which is about 2.3 V vs Mg/Mg^{2+} (Figure 2b). If the cell is operated beyond 2.3 V vs Mg/Mg^{2+}, a higher capacity and voltage would be expected; but, in this region, the cell would operate under a Daniell-type mechanism with anions acting as the ionic carrier. We note there are other possible Mg electrolytes available, including MACC,[30] alkoxide,[46] and carborane, among others,[47] which might also function well in the rocking-chair configuration.

To compare the TFSI-based electrolyte with the Grignard-based electrolyte, AC/Mg coin cells were fabricated with three different Mg electrolytes: Grignard-based all-phenyl complex (APC) electrolyte without and with the addition of LiCl and the TFSI-based electrolyte. The coin cells were cycled galvanostatically within 0.2−2.0 V at 50 μA cm^{-2} (Figure 5a).

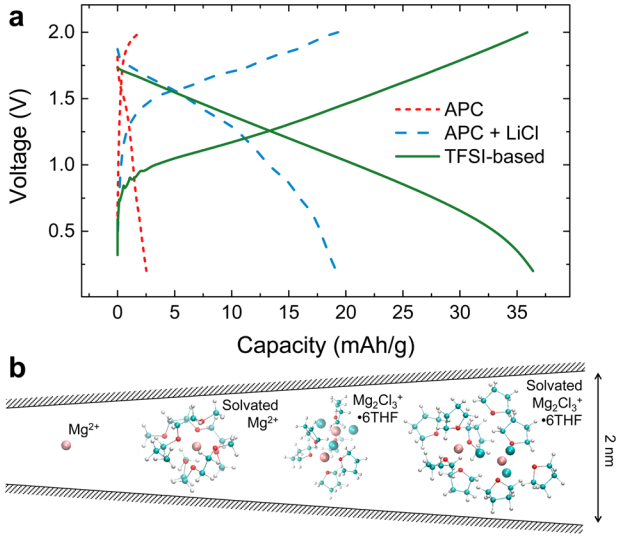

Figure 5. (a) Galvanostatic charge−discharge profiles collected in coin-type AC/Mg cells with different electrolytes: Grignard-based APC solution (red dots), APC solution saturated with Li-ion (blue dash), and the TFSI-based Mg^{2+} electrolyte solution (green line). (b) Comparison of the size of solvated and desolvated Mg-ions with respect to the micropore size of AC: Mg^{2+} and $[Mg_2Cl_3{\cdot}6THF]^+$ ions in TFSI-based and Grignard-based electrolytes, respectively. Mg^{2+} and Cl^- are depicted in pink and green space-filling format, respectively, and diglyme and THF are depicted in ball and stick format.

Coin-type cells with pure APC electrolyte show negligible capacity of 2.5 mAh g^{-1}, which corresponds to 5.6 F g^{-1}. The coin-type cells with APC electrolyte saturated with LiCl show 19.2 mAh g^{-1}, which corresponds to 43.2 F g^{-1}. As the coin-type cells can accommodate limited volume of electrolyte (ca. 200 μL), the cells that depend on the Daniell-type mechanism show limited capacity because of the depletion of active ions. On the other hand, coin-type cells made with TFSI-based electrolyte show the capacity of 36.4 mAh g^{-1}, which corresponds to 104.5 F g^{-1}, with a linear voltage profile that is a representative characteristic of supercapacitors. Even though limited volume of electrolyte is used, the rocking-chair-type mechanism makes the normal operation possible for the coin-type cells made with TFSI-based Mg^{2+} electrolyte.

Molecular dynamics (MD) simulations revealed a significant difference in the size of magnesium ions in Grignard- and TFSI-based electrolytes (Figure 5b). The diameter of $[Mg_2Cl_3{\cdot}6THF]^+$ cations in Grignard-based electrolytes is found to be ca. 12.85 Å, and the solvated diameter can reach 18.5 Å. On the other hand, the diameter of solvated Mg^{2+} cations with diglymes in a TFSI-based electrolyte is calculated to be about 10 Å, whereas the diameter of Mg^{2+} cation itself is 1.72 Å.[48] Since the pore size of the AC is less than 20 Å,[49] pores in AC can barely accommodate magnesium ions in Grignard-based electrolytes, in contrast to TFSI-based electrolytes. This finding

DOI: 10.1021/acsami.6b08367
ACS Appl. Mater. Interfaces 2016, 8, 30853−30862

explains the different electrochemical behavior of the corresponding electrochemical cells (Figure 5a).

Self-discharge is also one of the limiting factors in the application of supercapacitors.[50] In the case of conventional supercapacitors, large leakage currents can lead to severe losses such that ~30% of the initial capacity is retained after 72 h.[51−53] These leakage currents originate from faradaic reactions that make AC electrodes nonideally polarizable as potentials are set far above or far below the pzc upon charging.[54−56] On the contrary, for the rocking-chair-type metal hybrid supercapacitors, the charging cutoff potential of the AC electrode is pinned to the potential close to pzc, which was ~2.3 V vs Mg/Mg^{2+} in this case. Therefore, one can expect significantly reduced leakage current and self-discharge in rocking-chair-type supercapacitors. Figure 6 shows that 94% and 98% retention of potential was observed in the AC electrode after 72 h under open circuit conditions when charging was stopped at 2.7 and 2.2 V vs Mg/Mg^{2+}, respectively. This result supports our hypothesis and evidences substantially lower self-discharge compared to conventional supercapacitors.

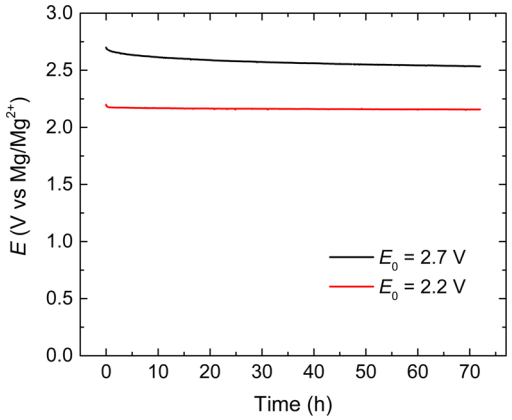

Figure 6. Trends of open circuit potential over the rest time of 72 h at 25 °C for AC electrode after charging at 2.7 V (black) and 2.2 V (red) vs Mg/Mg^{2+}. The potential was measured with respect to Mg metal as the reference electrode in a 3-electrode cell.

We also studied the cycling performance of the Mg hybrid supercapacitor in coin-type cells. Figure 7a shows that 64% of the initial capacitance was retained after 400 cycles at 1 mA cm^{-2}. To study the properties of cathode and anode separately, we cycled the hybrid supercapacitor in a 3-electrode configuration (Figure 7b). The discharging voltage profiles of the AC cathode (black lines in Figure 7b) show that the capacitance at potentials higher than 1.7 V vs Mg/Mg^{2+} is nearly constant during cycling; most of the capacitance fade occurs at lower potentials. A plausible explanation for this effect is the trapping of Mg^{2+} ions in the electrode pores,[42,57] which is consistent with the doorknob-shaped voltammogram (Figure 2b).[43] The voltage hysteresis for the desorption process in Figure 2b also evidences the difficulties of removing the trapped Mg^{2+} ions at low potentials. Remarkably, the Mg metal anode (red lines in Figure 7b) exhibits stable operation up to 300 cycles with an overpotential of 0.23 V, while the potential rises notably to 0.4−0.9 V vs Mg/Mg^{2+} beyond 300 cycles. The increase in overpotential may be associated with the thermodynamic instability of $TFSI^-$ ion at the low potentials.[36,58] Optimizing the electrolyte may alleviate both of the issues, capacitance fading at an AC cathode and overpotential at a Mg anode.

To further establish the metal hybrid supercapacitors concept, we also evaluated an AC/Zn cell with a TFSI-based Zn^{2+} electrolyte. The TFSI-based Zn^{2+} electrolyte possesses about ten times higher ionic conductivity compared to the TFSI-based Mg^{2+} electrolyte (i.e., 28.3 vs 3.2 mS cm^{-1}) and exhibits more than 99% Coulombic efficiency for Zn deposition and stripping.[27] Figure 8a shows that both the charge and discharge voltage profiles were linear even at 5 mA cm^{-2}, above which the operation of the Mg hybrid capacitor was limited due to the emergence of large overpotentials. The box-shaped cyclic voltammogram from the AC electrode (Figure 8b) is indicative of facile adsorption/desorption kinetics, and the electrode exhibits near ideal behavior as a supercapacitor.[59] A local minimum in the current at 0.7 V vs Zn/Zn^{2+} is associated with the pzc of the AC electrode. The presence of this pzc means that the rocking chair-type mechanism holds below 0.7 V. The narrower voltage range for this mechanism of operation arises from the fact that the redox potential of Zn metal is higher than Mg by 1.6 V. Since the cell was operated up to 1.8 V vs Zn/

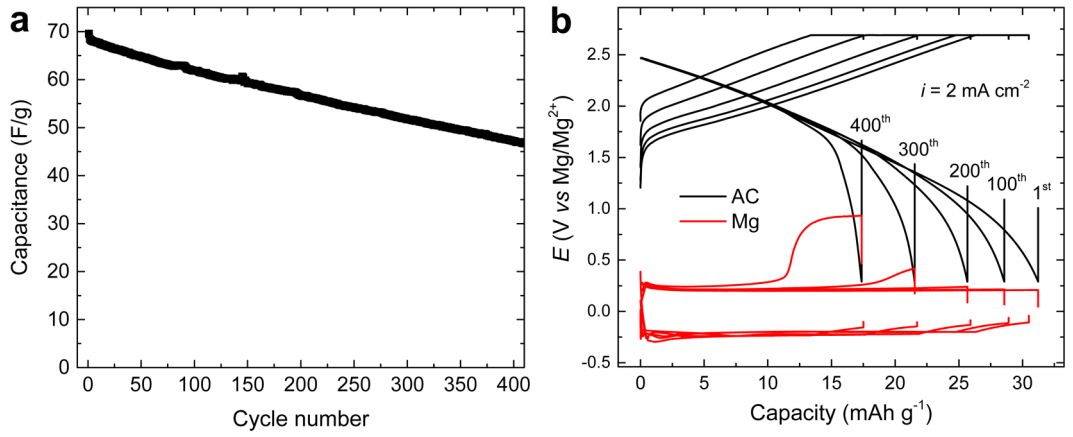

Figure 7. (a) Cycling performance of a coin-type AC/Mg cell with the TFSI-based electrolyte between 1.0 and 2.1 V at current density of 1.0 mA cm^{-2}. Upon charging, the voltage of the cell was held at 2.1 V until the current dropped from 1.0 to 0.5 mA cm^{-2}. (b) Plot of the voltage profiles of both electrodes upon multiple cycles in a 3-electrode cell. Upon charging, the voltage of the cell was held at 2.7 V vs Mg/Mg^{2+} until the current dropped from 2.0 to 0.4 mA cm^{-2}.

DOI: 10.1021/acsami.6b08367
ACS Appl. Mater. Interfaces 2016, 8, 30853−30862

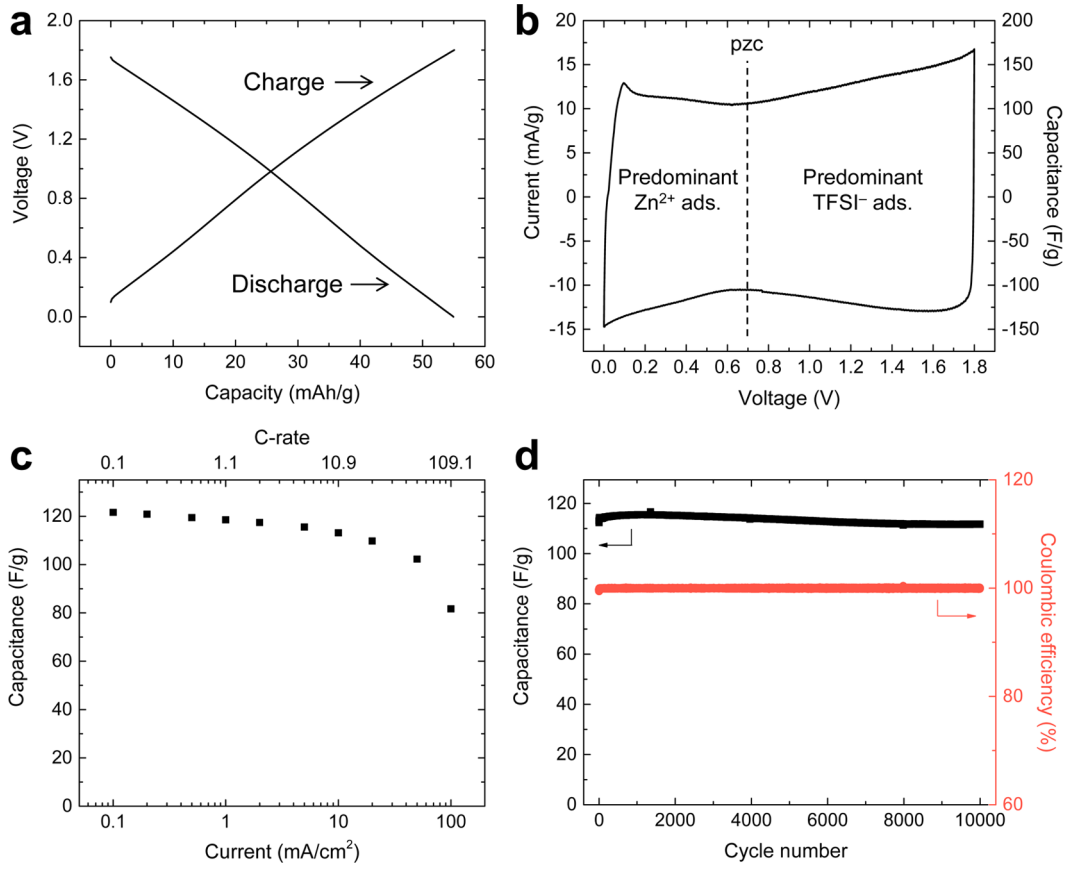

Figure 8. Electrochemical performance of Zn hybrid supercapacitor cells: (a) voltage profile at 5 mA cm^{-2}, (b) cyclic voltammogram at 0.1 mV s^{-1}, (c) galvanostatic rate performance, and (d) cycle performance at 5 mA cm^{-2}.

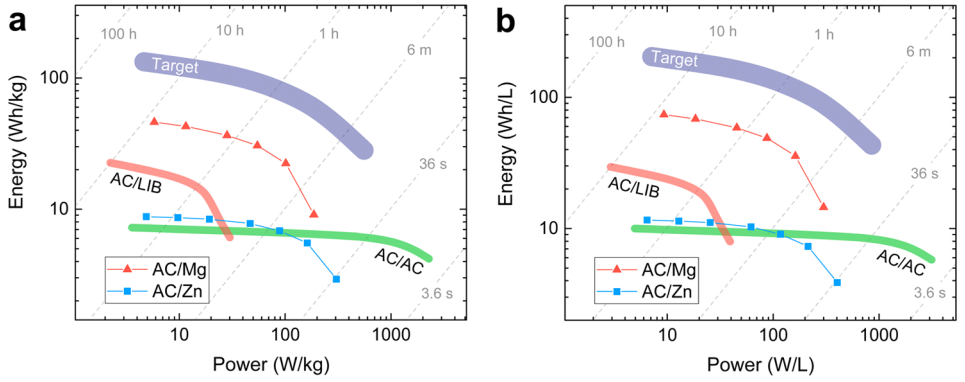

Figure 9. Ragone plot for Mg and Zn hybrid capacitors compared with conventional electric double-layer capacitors (AC/AC) and lithium-ion hybrid capacitor (AC/LIB) in terms of (a) mass-specific and (b) volumetric energy and power. The highest predicted limit of energy and power densities of ideal metal hybrid capacitors is plotted as "Target".

Zn^{2+} and this value is positive of the pzc, anionic adsorption starts to predominate at above 0.7 V vs Zn/Zn^{2+}. Quantitatively, this approach implies that about 60% of the ions are stored through the Daniell-type mechanism, thus depleting/replenishing ions from/to the electrolyte. Nonetheless, the high ionic conductivity of the electrolyte leads to a high rate capability that preserves 80 F g^{-1} at 100 mA cm^{-2}, where the charge or discharge takes place in 33 s (Figure 8c). Above 98% of the initial capacitance was retained after 10 000 cycles (Figure 8d), which is due to the facile adsorption/desorption kinetics and the excellent stability of the electrolyte against Zn metal. The AC/Zn cell is an exemplary system that has a highly conductive electrolyte wherein the metal anode is completely stable. The example of the AC/Zn system justifies the promise that other metal hybrid supercapacitors could be designed with high rate and cycle performances through judicious engineering of the components of the cell and its design.

The energy densities of the "rocking-chair"-type metal hybrid supercapacitor cells were estimated to be about 72.9 Wh L^{-1} (45.5 Wh kg^{-1}) and 11.6 Wh L^{-1} (8.7 Wh kg^{-1}) for AC/Mg and AC/Zn cells, respectively. The AC/Zn cell has similar energy density compared to the AC/AC cell because of the high redox potential of the Zn metal anode. On the other hand, the values for the AC/Mg cell exceed that of conventional AC/AC symmetric supercapacitors (9.9 Wh L^{-1} or 7.2 Wh kg^{-1}) by a factor of 7. Also, the AC/Mg hybrid supercapacitor shows 2.4

DOI: 10.1021/acsami.6b08367
ACS Appl. Mater. Interfaces 2016, 8, 30853−30862

Table 1. Comparison of Specific Energy and Energy Density of Nonaqueous Supercapacitors Calculated on the Basis of Different Configurations and the Operating Mechanism

configuration	AC|AC	AC|Li_xC_6	AC|Zn		AC|Mg	
mechanism[a]	D	D	R-C	R-C+D	R-C	R-C+D
energy density (Wh L^{-1})	9.9	29.3	5.9	11.6	62.3	73.8
specific energy (Wh kg^{-1})	7.2	22.5	3.7	8.8	39.0	46.2

[a]D: Daniell-type; R-C: rocking-chair-type; R-C+D: rocking-chair-type with additional Daniell-type.

times larger energy density and an order of magnitude higher power density compared to AC/Li_xC_6 asymmetric supercapacitors that has 29.3 Wh L^{-1} or 22.5 Wh kg^{-1} (Figure 9 and Table 1). Note that the values were calculated on the basis of the mass and volume of both the electrodes and the electrolyte. This increase is due to the large specific and volumetric capacity of metal electrodes and the decrease in the necessary amount of electrolyte. These properties are especially beneficial for high-end supercapacitors that have to provide energy in volume-restricted applications such as electric vehicles. Importantly, the abundance of main elements (i.e., Mg, Zn, and C) implies that these metal hybrid supercapacitors could be competitive for scale-up in large scale applications.[57,60−63]

Further development of new electrolytes and porous electrodes will bring about advanced metal hybrid supercapacitors with enhanced energy density, cyclability, and rate capability. For instance, optimizing the microporous carbon electrodes can increase the capacitance.[64] Functionalization by *p*-doping of the activated carbon can increase the pzc by about 300 mV[65] which, in turn, increases the voltage range where the rocking chair-type mechanism holds. Metal electrodes with lower redox potentials such as Li and Na have reduction potentials 2.5−3.0 V below the pzc of AC. Given these potentials, we could expect a hybrid supercapacitor device to attain up to 203.8 Wh L^{-1} (132.7 Wh kg^{-1}) together with excellent power capability (Figure 9), which would make these environmentally benign devices transcend Ni−Cd or lead-acid batteries.

CONCLUSIONS

Divalent metal and activated carbon electrodes were combined with new TFSI-based electrolytes to build hybrid supercapacitors that follow a "rocking-chair"-type mechanism. The "rocking-chair"-type mechanism overcomes the inherent limitation in energy density of conventional supercapacitors that follow a Daniell-type mechanism, that is, the need to introduce large volume of electrolyte to preserve internal resistance. The constant internal resistance with respect to different voltages validated the "rocking-chair"-type mechanism of these metal hybrid supercapacitors. The electrochemical reactions of metal and AC electrodes were highly reversible. The Mg hybrid supercapacitor achieved 90 F g^{-1} up to 2.6 V vs Mg/Mg^{2+}, resulting in a large energy density of 72.9 Wh L^{-1}, 7-fold larger than conventional supercapacitors. As AC electrodes are fully charged near pzc for Mg hybrid supercapacitor, the leakage current was substantially alleviated compared to conventional supercapacitors; the self-discharge was less than 6% after 72 h. Extended cycling at high current density led to fading in capacitance, which was attributed to the trapping of Mg^{2+} ions in the small micropores of the AC cathode and the degradation of the Mg metal anode. However, the excellent rate and cycle performance achieved with Zn hybrid supercapacitor evidence that improvements can be brought about by more stable and conductive electrolytes. It also highlights the very fast kinetics of plating/stripping in these divalent metal electrodes, which could also be used in high energy batteries if appropriate cathodes are discovered. The "rocking-chair"-type hybrid supercapacitors offer a new path forward toward higher energy density and high power supercapacitors, through both the exploration of new chemistries and optimization of the device construction to minimize unutilized materials.

AUTHOR INFORMATION

Corresponding Authors

*E-mail: jcabana@uic.edu (J. Cabana).
*E-mail: knecht9@uic.edu (H.D. Yoo).

Notes

The authors declare no competing financial interest.

ACKNOWLEDGMENTS

This work was supported as part of the Joint Center for Energy Storage Research (JCESR), an Energy Innovation Hub funded by the U.S. Department of Energy (DOE), Office of Science, Basic Energy Sciences (BES). Computational resources for this research were provided by the National Energy Research Scientific Computing Center, which is supported by the Office of Science of the U.S. Department of Energy under Contract No. DE-AC02-05CH11231.

REFERENCES

(1) Dunn, B.; Kamath, H.; Tarascon, J.-M. Electrical Energy Storage for the Grid: A Battery of Choices. *Science* **2011**, *334* (6058), 928−935.

(2) Kurzweil, P. Capacitors | Electrochemical Double-Layer Capacitors. In *Encyclopedia of Electrochemical Power Sources*; Garche, J., Ed.; Elsevier: Amsterdam, 2009; pp 607−633.

(3) Pandolfo, A. G.; Hollenkamp, A. F. Carbon Properties and Their Role in Supercapacitors. *J. Power Sources* **2006**, *157* (1), 11−27.

(4) Burke, A., Capacitors | Application. In *Encyclopedia of Electrochemical Power Sources*; Garche, J., Ed.; Elsevier: Amsterdam, 2009; pp 685−694.

(5) Yoo, H. D.; Shterenberg, I.; Gofer, Y.; Doe, R. E.; Fischer, C. C.; Ceder, G.; Aurbach, D. A Magnesium-Activated Carbon Hybrid Capacitor. *J. Electrochem. Soc.* **2014**, *161* (3), A410−A415.

(6) Yagi, S.; Ichitsubo, T.; Shirai, Y.; Yanai, S.; Doi, T.; Murase, K.; Matsubara, E. A Concept of Dual-Salt Polyvalent-Metal Storage Battery. *J. Mater. Chem. A* **2014**, *2* (4), 1144−1149.

(7) Zheng, J. P. The Limitations of Energy Density of Battery/Double-Layer Capacitor Asymmetric Cells. *J. Electrochem. Soc.* **2003**, *150* (4), A484−A492.

(8) Zheng, J. P. Theoretical Energy Density for Electrochemical Capacitors with Intercalation Electrodes. *J. Electrochem. Soc.* **2005**, *152* (9), A1864−A1869.

(9) Zheng, J. P. High Energy Density Electrochemical Capacitors without Consumption of Electrolyte. *J. Electrochem. Soc.* **2009**, *156* (7), A500−A505.

(10) Yoo, H. D.; Liang, Y.; Li, Y.; Yao, Y. High Areal Capacity Hybrid Magnesium−Lithium-Ion Battery with 99.9% Coulombic Efficiency for Large-Scale Energy Storage. *ACS Appl. Mater. Interfaces* **2015**, *7* (12), 7001−7007.

DOI: 10.1021/acsami.6b08367
ACS Appl. Mater. Interfaces 2016, 8, 30853−30862

(11) Pell, W. G.; Conway, B. E.; Marincic, N. Analysis of Non-Uniform Charge/Discharge and Rate Effects in Porous Carbon Capacitors Containing Sub-Optimal Electrolyte Concentrations. *J. Electroanal. Chem.* **2000**, *491* (1−2), 9−21.
(12) Du Pasquier, A.; Plitz, I.; Menocal, S.; Amatucci, G. A Comparative Study of Li-Ion Battery, Supercapacitor and Nonaqueous Asymmetric Hybrid Devices for Automotive Applications. *J. Power Sources* **2003**, *115* (1), 171−178.
(13) Pell, W. G.; Conway, B. E. Peculiarities and Requirements of Asymmetric Capacitor Devices Based on Combination of Capacitor and Battery-Type Electrodes. *J. Power Sources* **2004**, *136* (2), 334−345.
(14) Wang, Y.-g.; Xia, Y.-y. A New Concept Hybrid Electrochemical Surpercapacitor: Carbon/$LiMn_2O_4$ Aqueous System. *Electrochem. Commun.* **2005**, *7* (11), 1138−1142.
(15) Fan, L. Z.; Hu, Y. S.; Maier, J.; Adelhelm, P.; Smarsly, B.; Antonietti, M. High Electroactivity of Polyaniline in Supercapacitors by Using a Hierarchically Porous Carbon Monolith as a Support. *Adv. Funct. Mater.* **2007**, *17* (16), 3083−3087.
(16) Kurzweil, P. Capacitors | Electrochemical Hybrid Capacitors. In *Encyclopedia of Electrochemical Power Sources*; Garche, J., Ed.; Elsevier: Amsterdam, 2009; pp 658−664.
(17) Cericola, D.; Novák, P.; Wokaun, A.; Kötz, R. Hybridization of Electrochemical Capacitors and Rechargeable Batteries: An Experimental Analysis of the Different Possible Approaches Utilizing Activated Carbon, $Li_4Ti_5O_{12}$ and $LiMn_2O_4$. *J. Power Sources* **2011**, *196* (23), 10305−10313.
(18) Naoi, K.; Ishimoto, S.; Miyamoto, J.-i.; Naoi, W. Second Generation 'Nanohybrid Supercapacitor': Evolution of Capacitive Energy Storage Devices. *Energy Environ. Sci.* **2012**, *5* (11), 9363−9373.
(19) Come, J.; Augustyn, V.; Kim, J. W.; Rozier, P.; Taberna, P.-L.; Gogotsi, P.; Long, J. W.; Dunn, B.; Simon, P. Electrochemical Kinetics of Nanostructured Nb_2O_5 Electrodes. *J. Electrochem. Soc.* **2014**, *161* (5), A718−A725.
(20) Lim, E.; Kim, H.; Jo, C.; Chun, J.; Ku, K.; Kim, S.; Lee, H. I.; Nam, I.-S.; Yoon, S.; Kang, K.; Lee, J. Advanced Hybrid Supercapacitor Based on a Mesoporous Niobium Pentoxide/Carbon as High-Performance Anode. *ACS Nano* **2014**, *8* (9), 8968−8978.
(21) Zhao, E.; Qin, C.; Jung, H.-R.; Berdichevsky, G.; Nese, A.; Marder, S.; Yushin, G. Lithium Titanate Confined in Carbon Nanopores for Asymmetric Supercapacitors. *ACS Nano* **2016**, *10* (4), 3977−3984.
(22) Ling, C.; Banerjee, D.; Matsui, M. Study of the Electrochemical Deposition of Mg in the Atomic Level: Why It Prefers the Non-Dendritic Morphology. *Electrochim. Acta* **2012**, *76*, 270−274.
(23) Matsui, M. Study on Electrochemically Deposited Mg Metal. *J. Power Sources* **2011**, *196* (16), 7048−7055.
(24) Ha, S.-Y.; Lee, Y.-W.; Woo, S. W.; Koo, B.; Kim, J.-S.; Cho, J.; Lee, K. T.; Choi, N.-S. Magnesium(II) Bis(Trifluoromethane Sulfonyl) Imide-Based Electrolytes with Wide Electrochemical Windows for Rechargeable Magnesium Batteries. *ACS Appl. Mater. Interfaces* **2014**, *6* (6), 4063−4073.
(25) Cheng, Y.; Stolley, R. M.; Han, K. S.; Shao, Y.; Arey, B. W.; Washton, N. M.; Mueller, K. T.; Helm, M. L.; Sprenkle, V. L.; Liu, J.; Li, G. Highly Active Electrolytes for Rechargeable Mg Batteries Based on a $[Mg_2(\mu\text{-}Cl)_2]^{2+}$ Cation Complex in Dimethoxyethane. *Phys. Chem. Chem. Phys.* **2015**, *17* (20), 13307−13314.
(26) Shterenberg, I.; Salama, M.; Yoo, H. D.; Gofer, Y.; Park, J.-B.; Sun, Y.-K.; Aurbach, D. Evaluation of $(CF_3SO_2)_2N^-$ (TFSI) Based Electrolyte Solutions for Mg Batteries. *J. Electrochem. Soc.* **2015**, *162* (13), A7118−A7128.
(27) Han, S.-D.; Rajput, N. N.; Qu, X.; Pan, B.; He, M.; Ferrandon, M. S.; Liao, C.; Persson, K. A.; Burrell, A. K. Origin of Electrochemical, Structural and Transport Properties in Nonaqueous Zinc Electrolytes. *ACS Appl. Mater. Interfaces* **2016**, *8* (5), 3021−3031.
(28) Ichitsubo, T.; Okamoto, S.; Kawaguchi, T.; Kumagai, Y.; Oba, F.; Yagi, S.; Goto, N.; Doi, T.; Matsubara, E. Toward "Rocking-Chair Type" Mg-Li Dual-Salt Batteries. *J. Mater. Chem. A* **2015**, *3*, 10188−10194.
(29) Sa, N.; Pan, B.; Saha-Shah, A.; Hubaud, A. A.; Vaughey, J. T.; Baker, L. A.; Liao, C.; Burrell, A. K. Role of Chloride for a Simple, Non-Grignard Mg Electrolyte in Ether-Based Solvents. *ACS Appl. Mater. Interfaces* **2016**, *8* (25), 16002−16008.
(30) See, K. A.; Chapman, K. W.; Zhu, L.; Wiaderek, K. M.; Borkiewicz, O. J.; Barile, C. J.; Chupas, P. J.; Gewirth, A. A. The Interplay of Al and Mg Speciation in Advanced Mg Battery Electrolyte Solutions. *J. Am. Chem. Soc.* **2016**, *138* (1), 328−337.
(31) Mizrahi, O.; Amir, N.; Pollak, E.; Chusid, O.; Marks, V.; Gottlieb, H.; Larush, L.; Zinigrad, E.; Aurbach, D. Electrolyte Solutions with a Wide Electrochemical Window for Recharge Magnesium Batteries. *J. Electrochem. Soc.* **2008**, *155* (2), A103−A109.
(32) Lu, Z.; Schechter, A.; Moshkovich, M.; Aurbach, D. On the Electrochemical Behavior of Magnesium Electrodes in Polar Aprotic Electrolyte Solutions. *J. Electroanal. Chem.* **1999**, *466* (2), 203−217.
(33) Seo, D. M.; Borodin, O.; Balogh, D.; O'Connell, M.; Ly, Q.; Han, S.-D.; Passerini, S.; Henderson, W. A. Electrolyte Solvation and Ionic Association III. Acetonitrile-Lithium Salt Mixtures−Transport Properties. *J. Electrochem. Soc.* **2013**, *160* (8), A1061−A1070.
(34) Ponrouch, A.; Frontera, C.; Barde, F.; Palacin, M. R. Towards a Calcium-Based Rechargeable Battery. *Nat. Mater.* **2016**, *15*, 169−172.
(35) Abraham, M. J.; van der Spoel, D.; Lindahl, E.; Hess, B.; the GROMACS development team *GROMACS User Manual version 5.1.2*; 2016; www.gromacs.org.
(36) Rajput, N. N.; Qu, X.; Sa, N.; Burrell, A. K.; Persson, K. A. The Coupling between Stability and Ion Pair Formation in Magnesium Electrolytes from First-Principles Quantum Mechanics and Classical Molecular Dynamics. *J. Am. Chem. Soc.* **2015**, *137* (9), 3411−3420.
(37) Zhong, C.; Deng, Y.; Hu, W.; Qiao, J.; Zhang, L.; Zhang, J. A Review of Electrolyte Materials and Compositions for Electrochemical Supercapacitors. *Chem. Soc. Rev.* **2015**, *44* (21), 7484−7539.
(38) Lide, D. R., Ed. Physical Constants of Inorganic Compounds. In *CRC Handbook of Chemistry and Physics*, Internet Version 2005; CRC Press: Boca Raton, FL, 2005.
(39) Sivakkumar, S. R.; Nerkar, J. Y.; Pandolfo, A. G. Rate Capability of Graphite Materials as Negative Electrodes in Lithium-Ion Capacitors. *Electrochim. Acta* **2010**, *55* (9), 3330−3335.
(40) Yoo, H. D.; Jang, J. H.; Ryu, J. H.; Park, Y.; Oh, S. M. Impedance Analysis of Porous Carbon Electrodes to Predict Rate Capability of Electric Double-Layer Capacitors. *J. Power Sources* **2014**, *267*, 411−420.
(41) Ruch, P. W.; Kötz, R.; Wokaun, A. Electrochemical Characterization of Single-Walled Carbon Nanotubes for Electrochemical Double Layer Capacitors Using Non-Aqueous Electrolyte. *Electrochim. Acta* **2009**, *54* (19), 4451−4458.
(42) Aurbach, D.; Levi, M. D.; Salitra, G.; Levy, N.; Pollak, E.; Muthu, J. Cation Trapping in Highly Porous Carbon Electrodes for EDLC Cells. *J. Electrochem. Soc.* **2008**, *155* (10), A745−A753.
(43) Mysyk, R.; Raymundo-Piñero, E.; Béguin, F. Saturation of Subnanometer Pores in an Electric Double-Layer Capacitor. *Electrochem. Commun.* **2009**, *11* (3), 554−556.
(44) Randles, J. E. B. Kinetics of Rapid Electrode Reactions. *Discuss. Faraday Soc.* **1947**, *1* (0), 11−19.
(45) Aurbach, D.; Lu, Z.; Schechter, A.; Gofer, Y.; Gizbar, H.; Turgeman, R.; Cohen, Y.; Moshkovich, M.; Levi, E. Prototype Systems for Rechargeable Magnesium Batteries. *Nature* **2000**, *407* (6805), 724−727.
(46) Pan, B.; Huang, J.; He, M.; Brombosz, S. M.; Vaughey, J. T.; Zhang, L.; Burrell, A. K.; Zhang, Z.; Liao, C. The Role of $MgCl_2$ as a Lewis Base in ROMgCl−$MgCl_2$ Electrolytes for Magnesium-Ion Batteries. *ChemSusChem* **2016**, *9* (6), 595−599.
(47) Tutusaus, O.; Mohtadi, R.; Arthur, T. S.; Mizuno, F.; Nelson, E. G.; Sevryugina, Y. V. An Efficient Halogen-Free Electrolyte for Use in Rechargeable Magnesium Batteries. *Angew. Chem., Int. Ed.* **2015**, *54* (27), 7900−7904.
(48) Shannon, R. Revised Effective Ionic Radii and Systematic Studies of Interatomic Distances in Halides and Chalcogenides. *Acta Crystallogr., Sect. A: Cryst. Phys., Diffr., Theor. Gen. Crystallogr.* **1976**, *32* (5), 751−767.

DOI: 10.1021/acsami.6b08367
ACS Appl. Mater. Interfaces 2016, 8, 30853−30862

(49) Elazari, R.; Salitra, G.; Garsuch, A.; Panchenko, A.; Aurbach, D. Sulfur-Impregnated Activated Carbon Fiber Cloth as a Binder-Free Cathode for Rechargeable Li-S Batteries. *Adv. Mater.* **2011**, *23* (47), 5641−5644.
(50) Tevi, T.; Yaghoubi, H.; Wang, J.; Takshi, A. Application of Poly (p-Phenylene Oxide) as Blocking Layer to Reduce Self-Discharge in Supercapacitors. *J. Power Sources* **2013**, *241*, 589−596.
(51) Ishikawa, M.; Morita, M.; Ihara, M.; Matsuda, Y. Electric Double-Layer Capacitor Composed of Activated Carbon Fiber Cloth Electrodes and Solid Polymer Electrolytes Containing Alkylammonium Salts. *J. Electrochem. Soc.* **1994**, *141* (7), 1730−1734.
(52) Ricketts, B. W.; Ton-That, C. Self-Discharge of Carbon-Based Supercapacitors with Organic Electrolytes. *J. Power Sources* **2000**, *89* (1), 64−69.
(53) Soavi, F.; Arbizzani, C.; Mastragostino, M. Leakage Currents and Self-Discharge of Ionic Liquid-Based Supercapacitors. *J. Appl. Electrochem.* **2014**, *44* (4), 491−496.
(54) Conway, B. E.; Pell, W. G.; Liu, T. C. Diagnostic Analyses for Mechanisms of Self-Discharge of Electrochemical Capacitors and Batteries. *J. Power Sources* **1997**, *65* (1), 53−59.
(55) Xu, K.; Ding, S. P.; Jow, T. R. Toward Reliable Values of Electrochemical Stability Limits for Electrolytes. *J. Electrochem. Soc.* **1999**, *146* (11), 4172−4178.
(56) Jang, J. H.; Yoon, S.; Ka, B. H.; Jung, Y.-H.; Oh, S. M. Complex Capacitance Analysis on Leakage Current Appearing in Electric Double-Layer Capacitor Carbon Electrode. *J. Electrochem. Soc.* **2005**, *152* (7), A1418−A1422.
(57) Yoo, H. D.; Shterenberg, I.; Gofer, Y.; Gershinsky, G.; Pour, N.; Aurbach, D. Mg Rechargeable Batteries: An On-Going Challenge. *Energy Environ. Sci.* **2013**, *6*, 2265−2279.
(58) Baskin, A.; Prendergast, D. Exploration of the Detailed Conditions for Reductive Stability of $Mg(TFSI)_2$ in Diglyme: Implications for Multivalent Electrolytes. *J. Phys. Chem. C* **2016**, *120* (7), 3583−3594.
(59) Biener, J.; Stadermann, M.; Suss, M.; Worsley, M. A.; Biener, M. M.; Rose, K. A.; Baumann, T. F. Advanced Carbon Aerogels for Energy Applications. *Energy Environ. Sci.* **2011**, *4* (3), 656−667.
(60) Mohtadi, R.; Mizuno, F. Magnesium Batteries: Current State of the Art, Issues and Future Perspectives. *Beilstein J. Nanotechnol.* **2014**, *5*, 1291−1311.
(61) Muldoon, J.; Bucur, C. B.; Gregory, T. Quest for Nonaqueous Multivalent Secondary Batteries: Magnesium and Beyond. *Chem. Rev.* **2014**, *114* (23), 11683−11720.
(62) Saha, P.; Datta, M. K.; Velikokhatnyi, O. I.; Manivannan, A.; Alman, D.; Kumta, P. N. Rechargeable Magnesium Battery: Current Status and Key Challenges for the Future. *Prog. Mater. Sci.* **2014**, *66*, 1−86.
(63) Crabtree, G. Perspective: The Energy-Storage Revolution. *Nature* **2015**, *526* (7575), S92−S92.
(64) Chmiola, J.; Yushin, G.; Gogotsi, Y.; Portet, C.; Simon, P.; Taberna, P. L. Anomalous Increase in Carbon Capacitance at Pore Sizes Less Than 1 Nanometer. *Science* **2006**, *313* (5794), 1760−1763.
(65) Cohen, I.; Avraham, E.; Noked, M.; Soffer, A.; Aurbach, D. Enhanced Charge Efficiency in Capacitive Deionization Achieved by Surface-Treated Electrodes and by Means of a Third Electrode. *J. Phys. Chem. C* **2011**, *115* (40), 19856−19863.

DOI: 10.1021/acsami.6b08367
ACS Appl. Mater. Interfaces 2016, 8, 30853−30862